Investigation of Structural and Magnetic Properties in Aluminium-Substituted Cobalt-Zinc Ferrite Metal Oxides

S. R. Sarve[1,a], K. G. Rewatkar[1,b], S. W. Awaghade[1,c], D. S. Bhowmick[2,d], A. N. Wazalwar[3,e], and P. B. Wasnik[3,f]

[1] *Vidya Vikas Arts Commerce & Science College, Samudrapur, Maharashtra, India.*
[2] *Arunrao Kalode Mahavidyalay, Nagpur, Maharashtra, India.*
[3] *Dr. Ambedkar College, Deekshabhoomi, Nagpur, Maharashtra, India.*

[a] sarve.sadanand@gmail.com
[b] kgrewatkar@gmail.com
[c] awaghadeshital87@gmail.com
[d] pakm.principal@gmail.com
[e] aartiwazalwar@yahoo.com
[f] pranaybwasnik@gmail.com

Abstract

In recent years, spinel ferrites have attracted considerable research interest due to their distinctive structural, magnetic and electrical properties, positioning them as promising candidates for a wide range of advanced technological applications. Aluminium substituted cobalt-zinc spinel ferrite with chemical composition $Co_{0.2}Zn_{0.8}Fe_{2-x}Al_xO_4$ (x = 0.0, 0.2, 0.4, 0.6, 0.8, 1.0) were synthesized by the sol-gel auto-combustion technique. The structural properties of the synthesized ferrites were studied by X-ray diffraction (XRD), Fourier transform infrared (FTIR) spectroscopy, energy dispersive X-ray (EDX) analysis, transmission electron microscopy (TEM) and magnetic properties were analyzed by vibrating sample magnetometry (VSM). XRD results confirmed the formation of a single-phase cubic spinel structure with a space group Fd-3m and particle sizes were in the range of 12 nm to 72 nm. The FTIR spectra showed distinct absorption bands around 570 cm^{-1} and 450 cm^{-1}, which were attributed to the stretching vibrations of metal-oxygen bonds at tetrahedral and octahedral sites, respectively. The magnetic studies demonstrated a progressive reduction in magnetic properties with increasing aluminium substitution concentration, culminating in the observation of superparamagnetic behavior at higher substitution levels. This behaviour is indicative of the significant influence of aluminium substitution on the magnetic characteristics of the material.

Keywords: Nano Size Ferrites, Spinel Structure, Sol-Gel Auto-Combustion, FTIR, VSM.
Received 29 January 2025; First Review 8 February 2025; Accepted 09 April 2025.

*** Address of correspondence**
S. R. Sarve
Vidya Vikas Arts Commerce & Science College, Samudrapur, Maharashtra, India.

Email: sarve.sadanand@gmail.com

How to cite this article
S. R. Sarve, K. G. Rewatkar, S. W. Awaghade, D. S. Bhowmick, Investigation of Structural and Magnetic Properties in Aluminium-Substituted Cobalt-Zinc Ferrite Metal Oxides, J. Cond. Matt. 2025; 03 (02): 100-106.

Available from:
https://doi.org/10.61343/jcm.v3i02.73

Introduction

Recently, metal-oxide nanoparticles have gained significant attention owing to their unique properties that distinguish them from bulk materials. Among these, spinel ferrites are particularly important in both industry and research because of their outstanding electrical and magnetic properties. Spinel ferrites have diverse applications in medicine, electronics, energy storage and environmental photocatalysis [1-3]. Zinc substituted cobalt ferrite nanoparticles are utilized in electronic devices such as transducers, transformers, and sensors due to their high magnetic, optical, and electrical properties [4-5]. Zinc ferrite nanomaterials with doped variants are the most suitable for magnetic hyperthermia therapy and targeted drug delivery because of their excellent biocompatibility and magnetic properties [6]. Therefore, research on non-magnetic doped cations in cobalt-zinc ferrite is crucial due to its potential benefits to society. Spinel-type ferrite is characterised by chemical formula MFe_2O_4 (M = Co, Ni, Mn, Mg, or different divalent cations) with interstitial tetrahedral (A) and octahedral (B) sites. The distribution of cations within these interstitial sites plays a crucial role in determining the essential properties of the ferrites [7-8]. Spinel ferrites are often categorized as normal, inverse or mixed depending on occupancy of divalent cations and Fe^{3+}

ions at interstitial sites. Mixed ferrites are regarded as important materials among these three categories due to their wide range of tunability in its properties. The spinel structure of $ZnFe_2O_4$ is normal, with all Fe^{3+} ions present in B sites and all Zn^{2+} ions in the A sites. In contrast, the spinel structure of $CoFe_2O_4$ is inverse, with Fe^{3+} ions distributed almost equally between the B and A sites and the Co^{2+} ions primarily in the B sites. Thus, cobalt zinc ferrite has a structure similar to mixed spinel [9-10]. The structural and magnetic characteristics of mixed spinel ferrites have been significantly impacted by the substitution of nonmagnetic Al^{3+} ions [11]. Over recent decades, multiple studies have been conducted to explore and enhance the magnetic and electrical properties of mixed ferrites through various synthesis techniques that involve substituting different divalent and trivalent cations. Several synthesis techniques, such as sol-gel auto-combustion [12], co-precipitation [13], hydrothermal [14], high-energy ball milling [15] and micro-emulsion [16] have been developed for synthesizing cobalt zinc ferrite nanoparticles. The sol-gel auto-combustion technique is particularly advantageous due to its ability to produce nanocrystallites with minimal contamination, low cost, high reactivity, straightforward processing and enhanced control over particle size and uniformity [17]. This study investigates the impact of aluminium substitution on the structural and magnetic properties of cobalt zinc ferrite ($Co_{0.2}Zn_{0.8}Fe_{2-x}Al_xO_4$, where x = 0.0, 0.2, 0.4, 0.6, 0.8, 1.0) synthesized via the sol-gel auto-combustion method. The synthesized samples were characterized using X-ray diffraction (XRD), transmission electron microscopy (TEM), energy-dispersive X-ray spectroscopy (EDX), Fourier transform infrared spectroscopy (FTIR), and vibrating sample magnetometry (VSM). The obtained results are systematically analysed and discussed in this paper. Overall, this study contributes valuable insights into the influence of Al doping on the properties of cobalt zinc ferrite, offering potential pathways for the customization of ferrites in various applications.

Method

Nanoparticles of aluminium-substituted cobalt zinc ferrite, with the chemical composition $Co_{0.2}Zn_{0.8}Fe_{2-x}Al_x O_4$ (where x = 0.0, 0.2, 0.4, 0.6, 0.8, 1.0), were synthesized using the sol-gel microwave assisted auto-combustion method. The precursor materials included cobalt nitrate hexahydrate, zinc nitrate hexahydrate, ferric nitrate nonahydrate and aluminium nitrate nonahydrate, all of analytical reagent (AR) grade with 99% purity, procured from Merck. Urea was used as a fuel in a stoichiometric ratio. The metal nitrates and urea were dissolved in deionized water to form a homogeneous gel solution, which was continuously stirred using a magnetic stirrer at 70°C until gel formation. The formed gel spontaneously ignited in a microwave oven, producing a loose powder. This powder was then finely ground using a mortar and pestle and annealed at 800°C for 4 hours to obtain the final nanoparticle phase.

The characterization of the synthesized samples was conducted using various analytical techniques. Fourier Transform Infrared Spectroscopy (FTIR) was performed using a Bruker 3000 Hyperion Microscope with a Vertex 80 FTIR System. Powder X-ray diffraction (XRD) analysis was carried out using Rigaku Miniflex 1800 with Cu-Kα radiation (operating at 40 kV and 15 mA) over a 2θ range of 10°–80°. For elemental microanalysis, a JEOL JSM-7600F Field Emission Gun-Scanning Electron Microscope (FEG-SEM) equipped with an Energy Dispersive X-ray Spectroscopy (EDS) detector was used. Transmission electron microscopy (TEM) was performed using Tecnai G2 F30 Field Emission Gun-Transmission Electron Microscope (FEG-TEM) operating at 300 kV for high-resolution imaging. Finally, magnetic measurements were conducted at room temperature using a Lakeshore 7410S Vibrating Sample Magnetometer (VSM).

Result and Discussion

FTIR Analysis

FTIR spectroscopy is a valuable technique for analysing cation distribution in spinel ferrites, as well as lattice vibrational modes. Figure 1 shows the infrared spectra of $Co_{0.2}Zn_{0.8}Fe_{2-x}Al_xO_4$ in frequency range 400-4000 cm^{-1}.

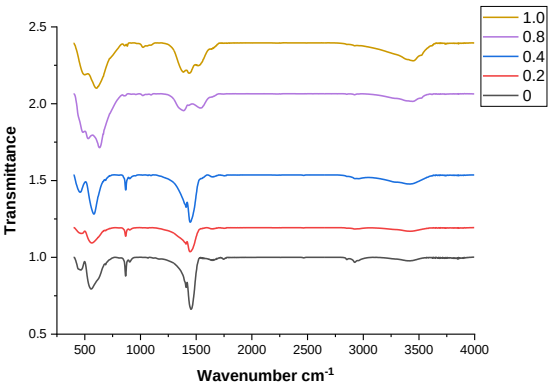

Figure 1: FT-IR spectrum of $Co_{0.2}Zn_{0.8}Fe_{2-x}Al_xO_4$.

Tetrahedral and octahedral clusters are identified by the existence of distinctive absorption bands in the frequency range of 450 cm^{-1} and 570cm^{-1}, that validate the stretching vibration resulting from interaction between the oxygen atom and cations in tetrahedral and octahedral sites in the spinel lattice structure [18]. The values of the corresponding bands have been presented in Table 1. It is found that both tetrahedral and octahedral vibrational frequencies shift towards higher frequencies as the Al^{3+} ions' concentration increases. This shift indicates changes in force constants and bond lengths within the lattice as well as the expansion

of sites due to cation migration among them. The following relation is used to calculate the force constant values.

$$K = 4\pi^2 c^2 \nu^2 \mu \qquad (1)$$

Where c = speed of light, ν denotes the vibrational frequency. The reduced mass μ is calculated by finding molecular weight of cations in octahedral sites, tetrahedral sites and oxygen atom. Where K_t and K_o is the force constant in accordance with both the sites i.e., tetrahedral and octahedral and K_a is the average force constant. In the Al-substituted cobalt zinc ferrite, we observe notable trends in band edge positions and force constants as shown in Table 1.

Table 1: The absorption bands (ν_1, ν_2) and force constant (K_t, K_0) in $Co_{0.2}Zn_{0.8}Fe_{2x}Al_xO_4$.

x	Position of band edge, cm^{-1}		Force constants, N/m		
	ν_1	ν_2	K_t	K_o	K_a
0	462.9	556.93	161.4	254.23	207.815
0.2	467.14	563.45	157.55	258.54	208.045
0.4	459.16	582.12	143.15	273.98	208.565
0.6	476.93	594.05	139.82	282.84	211.33
0.8	483.34	632.72	118.96	318.05	218.505
1	500.89	604.31	76.3	287.14	181.72

The low-frequency band (ν_1) fluctuates initially but generally increases, indicating changes in cation distribution and lattice dynamics, while the high-frequency band (ν_2) consistently rises, suggesting lattice stiffening due to Al^{3+} ions. The tetrahedral force constant (K_t) decreases significantly, implying weaker tetrahedral bonds as Fe^{3+} is replaced by Al^{3+}. The octahedral force constant (K_o) initially increases, peaking at x = 0.8, before decreasing, indicating structural imbalance. The average force constant (K_a) follows a similar trend. Moderate Al substitution (x ≈ 0.6 - 0.8) stabilizes the lattice, while excessive substitution weakens it.

X-RD Patterns Analysis

The X-ray diffraction patterns of Al-substituted cobalt-zinc ferrite ($Co_{0.2}Zn_{0.8}Fe_{2-x}Al_x O_4$; x = 0.0, 0.2, 0.4, 0.6, 0.8, 1.0) confirm the formation of a single-phase spinel ferrite structure. Figure 2 presents the diffraction patterns, where the most intense reflection is observed for the (311) plane, along with additional peaks corresponding to the (220), (400), (422), (511), and (440) planes. These characteristic reflections indicate the formation of a cubic spinel structure with the Fd-3m space group [19].

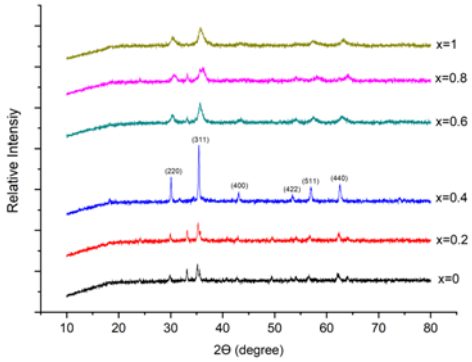

Figure 2: X-RD Pattern for $Co_{0.2}Zn_{0.8}Fe_{2-x}Al_xO_4$ (x = 0.0, 0.2, 0.4, 0.6, 0.8,1.0).

The absence of secondary phases suggests the successful incorporation of Al^{3+} ions into the ferrite lattice without disrupting its fundamental structure, making the material suitable for further investigation. All the peaks in the diffraction are indexed and refined by Powder X software. The crystallite size (D) of the samples was determined using the Debye-Scherrer equation (2).

$$D = \frac{0.89\lambda}{\beta \cos\theta} \qquad (2)$$

where λ is the X-ray wavelength, β represents the full-width at half-maximum (FWHM) of the (311) peak, and θ is the Bragg diffraction angle [20]. The calculated crystallite sizes for different compositions are presented in Table 2. The results show that crystallite size varies significantly with Al^{3+} substitution, initially increasing and then decreasing at higher concentrations.

Table 2: Structural parameters of $Co_{0.2}Zn_{0.8}Fe_{2-x}Al_xO_4$.

(x)	Crystallite size (nm)	Interplanar spacing d (A^0)	Lattice Constant a (A^0)	X-ray density ρ_m (g/cm^3)
x=0	47	2.5497	8.4566	0.3766
x= 0.2	48	2.5406	8.4263	0.3689
x= 0.4	72	2.5323	8.3987	0.3610
x= 0.6	17	2.5112	8.3288	0.3545
x= 0.8	12	2.4878	8.2513	0.3456
x= 1.0	13	2.5139	8.3379	0.3329

The initial increase in crystallite size (x = 0.4) suggests that Al^{3+} enhances grain growth up to a certain limit. The sharp decrease in crystallite size at x ≥ 0.6 indicates that excessive Al^{3+} substitution inhibits crystal growth, possibly due to

lattice distortion and increased strain. This trend implies that aluminium incorporation inhibits grain growth at higher concentrations by introducing lattice strain and increasing nucleation sites, resulting in finer crystallite sizes. The lattice constant (a), determined using interplanar spacing (d) through Bragg's law, shows a systematic decrease with increasing Al^{3+} concentration, as presented in Table 2. The observed contraction in lattice constant is attributed to the smaller ionic radius of Al^{3+} (0.59 Å) compared to Fe^{3+} (0.63 Å) [21]. As Fe^{3+} ions are progressively replaced by Al^{3+} ions, the shorter bond lengths lead to an overall reduction in lattice size. The slight increase at x = 1.0 suggests a possible rearrangement of cations within the spinel lattice. The X-ray density (ρ_x) was calculated using the formula:

$$\rho_x = \frac{8\,M}{N_A\,a^3} \qquad (3)$$

where M is the molecular weight of the sample, N_A is Avogadro's number, and a is the lattice parameter. The calculated X-ray density values, presented in Table 2, show a continuous decline with increasing Al^{3+} substitution. This continuous decrease in X-ray density is primarily due to the lower atomic weight of Al^{3+} (26.98 g/mol) compared to Fe^{3+} (55.85 g/mol). As Al^{3+} replaces Fe^{3+} in the lattice, the overall molecular weight of the unit cell decreases, leading to a corresponding reduction in X-ray density. This trend further confirms the successful incorporation of Al^{3+} ions into the ferrite structure and the associated lattice contraction. The XRD study indicate that moderate Al^{3+} substitution (x = 0.4–0.6) promotes crystallinity, while higher concentrations ($x \geq 0.8$) induce lattice distortion and grain refinement, affecting the overall microstructural stability of Co-Zn ferrite.

EDS Analysis

The elemental composition of aluminium-substituted cobalt zinc ferrites, was analysed using energy dispersive X-ray (EDS) spectroscopy.

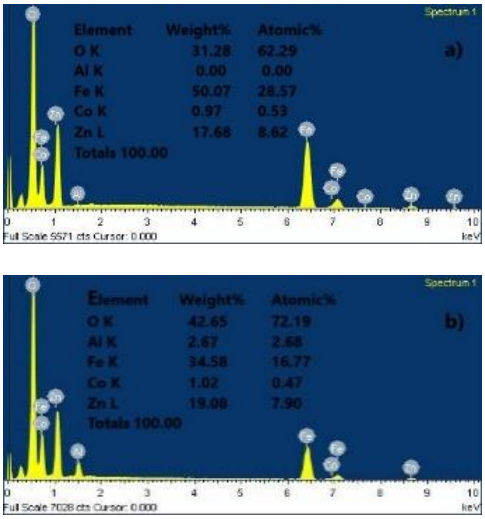

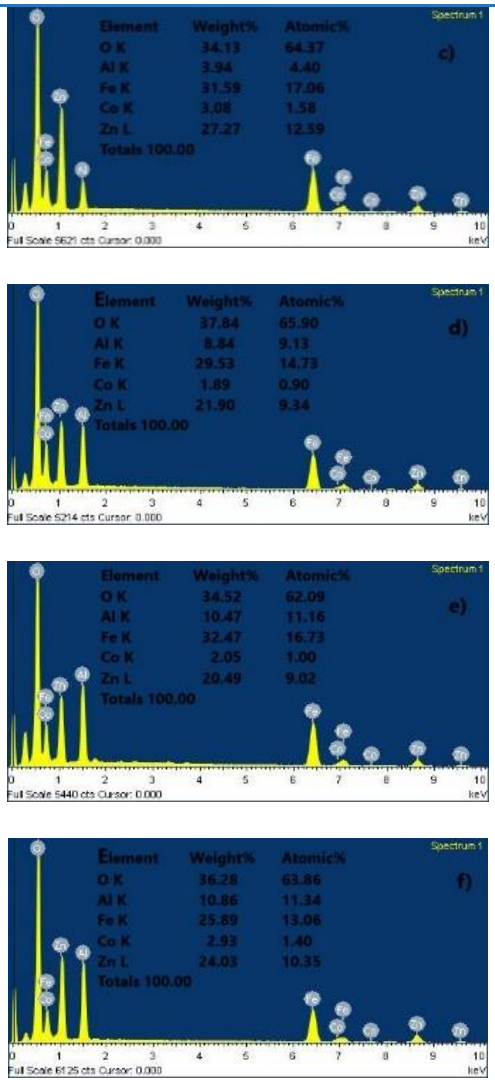

Figure 3: Energy dispersive X-ray analysis spectra of $Co_{0.2}Zn_{0.8}Fe_{2-x}Al_xO_4$ (a) x = 0 (b) x = 0.2 (c) x = 0.4 (d) x = 0.6 (e) x = 0.8 and (f) x = 1.00 samples.

The characteristic EDS spectra, shown in Figure 3(a)–(f), confirm the presence of Co, Zn, Fe, Al, and O elements, indicating the successful incorporation of aluminium into the ferrite lattice.

The experimentally obtained elemental percentages closely align with the nominal composition, validating the accuracy of the synthesis process. Furthermore, the absence of significant material loss or extraneous elements within the detection limits ensures the high purity and compositional integrity of the synthesized samples.

TEM Analysis

According to the HRTEM images, the obtained sample's particles are agglomerated and have a size that is entirely consistent with the information obtained from the X-RD investigations.

The agglomeration is due magnetic nature of the sample and large surface to volume ratio.

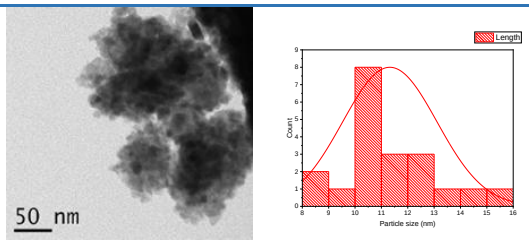

Figure 4: TEM Image of $Co_{0.2}Zn_{0.8}Fe_{2-x}Al_xO_4$ (x=0.6) and Histogram.

The Figure 4 indicates the HRTEM image of synthesised sample for the composition x=0.6 its particle size distribution histogram.

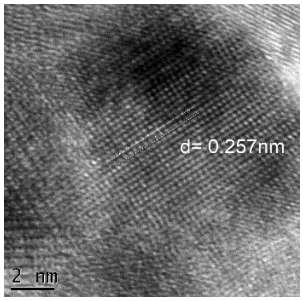

Figure 5: HR TEM Image of $Co_{0.2}Zn_{0.8}Fe_{2-x}Al_xO_4$ (x=1.0).

The Figure 5 gives the HRTEM image for the composition x= 1.0 at the scale of 2nm indicates the crystalline nature with interplanar spacing equal to 0.257nm, which is closely matched with the data of X-ray diffraction.

Magnetic Measurement

The typical hysteresis loop of $Co_{0.2}Zn_{0.8}Fe_{2-x}Al_xO_4$ with varying composition of x are shown in Figure.5 there is gradual decrease in saturation magnetization (M_S) from 5.444 emu/g to 1.799 emu/g with negligible value of coercivity (H_C) from 8.2353 Oe to 1.3504 Oe. The spinel ferrite's A-site and B-site cation occupancy and exchange interaction strength causes the variation in saturation magnetization (M_s).

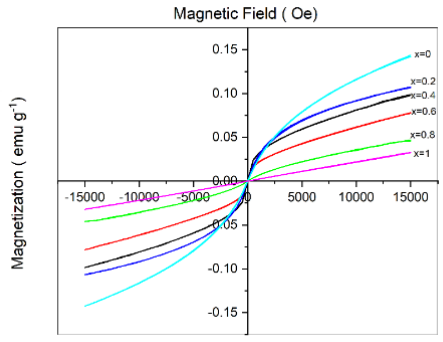

Figure 5: Hysteresis loop of $Co_{0.2}Zn_{0.8}Fe_{2-x}Al_xO_4$.

Tetrahedral A-site magnetism in spinel ferrite is anti-parallel to octahedral B-site magnetization. Neel's molecular field model indicates that A–B super-exchange interactions predominate over the A–A and B–B interactions [22].

The equation (4) provides net magnetic moment in ferrites.

$$n_B(x) = M_B(x) - M_A(x) \qquad (4)$$

The B- and A-sublattice magnetic moments in Bohr magneton (μB) are represented as $M_B(x)$ and $M_A(x)$, correspondingly. The saturation magnetization depends on the concentration of aluminium, and it is found that as aluminium' concentration increases, saturation magnetization decreases. The lower magnetic moment of the Al^{3+} ion relative to the Fe^{3+} ion (5μB) is the cause of this declining tendency. Based on particle sizes that ranged from 17nm to 12nm, the decline in saturation magnetization with x > 0.4 can also be elucidated. As the size of the grains increases, their contribution reduces, and Neel's two sub lattices indicate that the magnetization value surpasses the theoretical limit. The relationship between coercivity (Hc) and grain size can be understood through the domain structure, critical diameter, and crystal anisotropy. Due to thermal factors, coercivity in single domain region falls as grain size decreases. In single domain region, the coercivity H_c is given following equation.

$$H_c = g - \frac{h}{D^2} \qquad (5)$$

Where g and h are constants. 'D' represents particle diameter [23]. Even at the greatest applied magnetic fields, the single domain structure with superparamagnetic nature is indicated by the negligible values of coercive field and remanence magnetization (M_r) and the lack of full saturation.

Conclusion

The Aluminium-substituted Cobalt Zinc Ferrite, $Co_{0.2}Zn_{0.8}Fe_{2-x}Al_x O_4$ (x = 0.0, 0.2, 0.4, 0.6, 0.8, 1.0), was successfully synthesized using the sol-gel microwave-assisted auto-combustion method. The infrared spectrum, displaying fundamental peaks at 450 cm^{-1} and 570 cm^{-1}, confirms the formation of metal oxide bonds in the synthesized mixed ferrite. X-ray diffraction analysis identified a single-phase cubic spinel structure with the Fd-3m space group, exhibiting particle sizes ranging from 12 nm to 72 nm. Magnetic measurements reveal a superparamagnetic nature characterized by a single domain structure and a negligible coercivity value of 1.3504 Oe, particularly in particles as small as 12 nm. The study demonstrates that Aluminium substitution leads to lattice contraction and enhanced crystallinity up to an optimal concentration of x = 0.6; higher concentrations result in lattice distortion and inhibited crystal growth due to induced

stress and altered cation distributions. Furthermore, the non-magnetic nature of Aluminium dilutes the overall magnetic properties of the material, affecting saturation magnetization and coercivity. Thus, controlled Al^{3+} doping is essential for optimizing the structural and magnetic characteristics of ferrites, making it significant for tailored industrial applications.

Acknowledgement

The authors are grateful to Sophisticated Analytical Instrumentation Facility (SAIF) at the Indian Institutes of Technology in Bombay and Chennai for their essential support in the characterization of our synthesized samples. Their contributions were pivotal to the advancement of our research.

References

1. Hgjh Vinosha, P., Manikandan, A., Ceicilia, A., Dinesh, A., Nirmala, F., Preetha, A., Slimani, Y., Almessiere, M., Baykal, A., & Xavier, B. (2021), "*Review on recent advances of zinc substituted cobalt ferrite nanoparticles: Synthesis characterization and diverse applications",* Ceramics International, 47, 10512-10535. https://doi.org/10.1016/J.CERAMINT.2020.12.289.
2. Chahar, D., Taneja, S., Bisht, S., Kesarwani, S., Thakur, P., Thakur, A., & Sharma, P. (2021), *"Photocatalytic activity of cobalt substituted zinc ferrite for the degradation of methylene blue dye under visible light irradiation"*, Journal of Alloys and Compounds, 851, 156878. https://doi.org/10.1016/j.jallcom.2020.156878.
3. Sahoo, P., Choudhary, P., Laha, S., Dixit, A., & Mefford, O. (2023), *"Recent advances in zinc ferrite ($ZnFe_2O_4$) based nanostructures for magnetic hyperthermia applications"*, Chemical communications. https://doi.org/10.1039/d3cc01637d.
4. Jnaneshwara, D., Avadhani, D., Prasad, B., Nagabhushana, B., Nagabhushana, H., Sharma, S., Prashantha, S., & Shivakumara, C. (2014), *"Effect of zinc substitution on the nanocobalt ferrite powders for nanoelectronic devices"*, Journal of Alloys and Compounds, 587, 50-58. https://doi.org/10.1016/J.JALLCOM.2013.10.146.
5. Sathiyamurthy, K., Rajeevgandhi, C., Guganathan, L., Bharanidharan, S., & Savithiri, S. (2021), *"Enhancement of magnetic, supercapacitor applications and theoretical approach on cobalt-doped zinc ferrite nanocomposites"*, Journal of Materials Science: Materials in Electronics, 32, 11593 - 11606. https://doi.org/10.1007/s10854-021-05764-2.
6. Shaterabadi, Z., Nabiyouni, G., Asadi, Z., Iglesias, G., & Soleymani, M. (2023), *"Enhanced magnetic hyperthermia efficiency in poly vinyl alcohol-coated zinc-substituted cobalt ferrite nanoparticles: Correlated effects of zinc content and applied magnetic field strength"*, Ceramics International. https://doi.org/10.1016/j.ceramint.2023.08.088.
7. H S Ahamad, N. S. (2017), *"Structural properties of $Cu_xNi_{1-x}Fe_2O_4$ nano ferrites prepared by urea-gel microwave auto combustion method"*, Ferroelectrics, 516(1), 146-160. https://doi.org/10.1080/00150193.2017.1362285.
8. Sathiya Priya, D. G. (2019), *"Effect of Al substitution on the structural, electric and impedance behavior of cobalt ferrite"*, Vacuum, 160, 453-460. https://doi.org/10.1016/j.vacuum.2018.12.004.
9. Akshay B. Kulkarni, S. N. (2019), *"Variation in structural and mechanical properties of Cd-doped Co Zn ferrites"*, Volume 2, Issue 3,2019, Pages 455 462, ISSN 2589-2991, Materials Science for Energy Technologies, 2(3), 455-462. https://doi.org/10.1016/j.mset.2019.03.00.
10. N. N. Sarkar, S. A. (2019), *"Effect of Cobalt and Nickel Substitution on Structural and Magnetic Properties of Spinel Ferrite"*, Integrated Ferroelectrics, 203(1), 61 66. https://doi.org/10.1080/10.
11. Sathiya Priya, D. G. (2019), *"Effect of Al substitution on the structural, electric and impedance behavior of cobalt ferrite"*, Vacuum, 160, 453-460. https://doi.org/10.1016/j.vacuum.2018.12.004.
12. P. S. Hedaoo, D. B. (2019), *"Structural and Magnetic Studies of Zn Doped Nickel Nanoferrites Synthesize by Sol-gel Auto Combustion Method"*, Materials Today: Proceedings, 15(3), 416-423. https://doi.org/10.1016/j.matpr.2019.04.102.
13. Uzma, G., Ayesha, R., Zarfa, L, & Kainat, K. (2020). *"Effect of Synthesis Techniques on the Structural Properties of Cobalt doped Zinc Nano-Ferrites"*, International Journal of Engineering Research and, 9. https://doi.org/10.17577/IJERTV9IS030067.
14. Coppola, P., Silva, F., Gomide, G., Paula, F., Campos, A., Perzynski, R., Kern, C., Depeyrot, J., & Aquino, R. (2016), *"Hydrothermal synthesis of mixed zinc–cobalt ferrite nanoparticles: structural and magnetic properties"*, Journal of Nanoparticle Research, 18, 1-15. https://doi.org/10.1007/s11051-016-3430-1.
15. Sinha, M., & Pradhan, S. (2010), *"Synthesis of nanocrystalline Cd–Zn ferrite by ball milling and its stability at elevated temperatures"*, Journal of Alloys and Compounds, 489, 91-98.

https://doi.org/10.1016/J.JALLCOM.2009.09.019.
16. Viet, T., Hong, C., Quoc, T., & Dac, T. (2020), *"Study on synthesis and characterization of nano scale spinel $Mn_{0.5}Fe_{2.5}O_4$ by micro-emulsion method"*, Vietnam Journal of Catalysis and Adsorption. https://doi.org/10.51316/JCA.2020.066.
17. Tianfu, H., Qiu, Z., Hu, Z., & Lu, X. (2021), *"Novel method of preparing hierarchical porous $CoFe_2O_4$ by the citric acid-assisted sol-gel auto-combustion for supercapacitors",* Journal of energy storage, 35, 102286. https://doi.org/10.1016/J.EST.2021.102286.
18. Rathod, V., Anupama, A., Kumar, R., Jali, V., & Sahoo, B. (2017), *"Correlated vibrations of the tetrahedral and octahedral complexes and splitting of the absorption bands in FTIR spectra of Li-Zn ferrites"*, Vibrational Spectroscopy, 92, 267-272. https://doi.org/10.1016/J.VIBSPEC.2017.08.008.
19. Humbe, A., Kounsalye, J., Shisode, M., & Jadhav, K. (2017), *"Rietveld refinement, morphology and superparamagnetism of nanocrystalline $Ni_{0.70-x}Cu_xZn_{0.30}Fe_2O_4$ spinel ferrite"*, Ceramics International, 44, 5466-5472. https://doi.org/10.1016/J.CERAMINT.2017.12.180.
20. Cullity, B. D. (1976). Elements of X-raydiffraction. Addison-Wesley Publishing Co. Inc.
21. Ramesh, C., Maniysundar, K., & Selvanandan, S. (2016), *"Structural and magnetic study on al substituted MgZn mixed ferrite powders prepared by sol-gel method"*, Materials Today: Proceedings, 3, 1363-1369. https://doi.org/10.1016/J.MATPR.2016.04.016.
22. Smart, J. S. (1955). The Néel Theory of Ferrimagnetism. Am. J. Phys., 23(6), 356-370. https://doi.org/10.1119/1.1934006.
23. Li, Q., Kartikowati, C., Horie, S., Ogi, T., Iwaki, T., & Okuyama, K. (2017), *"Correlation between particle size/domain structure and magnetic properties of highly crystalline Fe_3O_4 nanoparticles"*, Scientific Reports, 7. https://doi.org/10.1038/s41598-017-09897-5.